UCRL-JC-134562
PREPRINT

Development of High-Energy Neutron Imaging for Use in NDE Applications

James Hall
Frank Dietrich
Clint Logan
Gregory Schmid

This paper was prepared for submittal to the
International Symposium on Optical Science,
Engineering, and Instrumentation
Denver, CO
July 18-23, 1999

June 1999

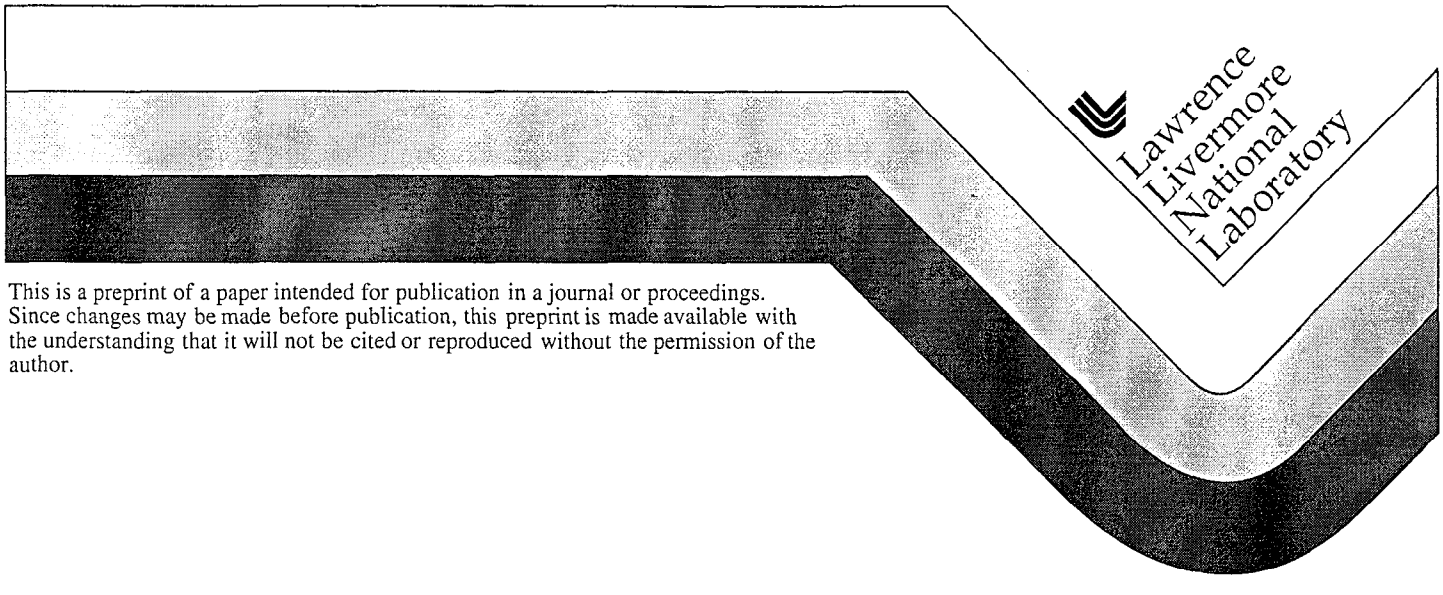

Development of high-energy neutron imaging for use in NDE applications

James Hall[a], Frank Dietrich, Clint Logan and Gregory Schmid

Lawrence Livermore National Laboratory

P.O. Box 808, M/S L-050, Livermore, CA 94551-9900

ABSTRACT

We are currently developing a high-energy (10 - 15 MeV) neutron imaging system for use in NDE applications. Our goal is to develop an imaging system capable of detecting cubic-mm-scale voids or other structural defects in heavily-shielded low-Z materials within thick sealed objects. The system will be relatively compact (suitable for use in a small laboratory) and capable of acquiring tomographic image data sets. The design of a prototype imaging detector and multi-axis staging system will be discussed and selected results from recent imaging experiments will be presented. The development of an intense, accelerator-driven neutron source suitable for use with the imaging system will also be discussed.

Keywords: neutron imaging, neutron radiography, computed tomography, non-destructive inspection, neutron sources

1. INTRODUCTION

Neutron imaging systems operating at thermal and fission spectrum energies ($\lesssim$ 2 MeV) are now well accepted as non-destructive inspection tools[1] with a number of academic and specialized industrial research facilities currently in operation in the U.S. and abroad;[2] however, the use of these systems is generally limited to the inspection of relatively thin objects (*i.e.* a few neutron mean free paths in total thickness). While references to neutron imaging at higher energies ($\gtrsim$ 8 MeV) have been relatively scarce in the literature until fairly recently,[3-22] we believe that this approach offers the potential to be a powerful technique for use in probing the internal structure of much thicker objects which may be essentially opaque to x rays and lower energy neutrons, particularly in situations where μm-scale spatial resolution is not required.

The project outlined here is an effort to develop high-energy neutron imaging to compliment (*not* replace) existing photon imaging techniques in NDE applications involving the inspection of thick sealed objects ($\rho x \gtrsim 100$ g/cm^2). In particular, our goal is to develop an imaging system capable of detecting cubic-mm-scale voids or other significant structural defects in heavily-shielded low-Z materials within such objects. The system that we are developing will be relatively compact (suitable for use in a small laboratory) and capable of acquiring tomographic image data sets. In order to expedite the overall development process and minimize associated technical risks, we are using commercially-available system components and proven neutron imaging techniques wherever possible. As currently envisioned, the imaging system will consist of an intense, accelerator-driven, D(d,n)^{3}He neutron source operating in the 10 - 15 MeV energy range with an equivalent yield $\approx 10^{12}/4\pi$ n/sec/sr along the beam axis and an effective spot size $\approx$ 1 – 1.5 mm (FWHM), a multi-axis staging system to support and manipulate the object under inspection (thereby allowing multiple angular views to be taken for tomographic imaging) and an imaging detector. The imaging detector itself will consist of a plastic scintillator ($\approx$ 60 cm X 60 cm) viewed indirectly by one or more cryogenically-cooled, high-resolution CCD cameras. The ultimate spatial resolution of the system (which depends on the source spot size, the intrinsic resolution of the detector and the overall imaging system magnification factor) is anticipated to be $\approx$ 0.80 – 1.10 mm (FWHM) at the object position.

The conceptual design of our proposed imaging system[23,24] and a description of several early "proof-of-principle" high-energy ($\approx$ 40 - 400 MeV) neutron imaging experiments carried out at the Los Alamos Nuclear Science Center (LANSCE)[15] which served to motivate the current work have already been presented elsewhere along with a discussion of the technical risks associated with developing and operating such a system (*e.g.* induced activation of specimens and radiation shielding requirements). In this paper, we will describe the design of a prototype imaging detector and multi-axis staging system proposed for use with the system and present selected results from recent imaging experiments. The parallel development of an intense neutron source suitable for use with the system will also be discussed.

[a] Email: jmhall@llnl.gov; Telephone: (925) 422-4468; Fax: (925) 423-3371

2. PROTOTYPE SYSTEM COMPONENTS

2.1 Imaging detector

The design of the imaging detector proposed for use in our system is based on proven U.S. Nuclear Test Program technology.[25] Our prototype for the detector consists of a rigid plastic scintillator viewed indirectly by a single commercial CCD camera. The camera assembly itself consists of a fast (f/1.00; 50 mm) photographic lens coupled through a remotely-controlled mechanical shutter housing to a thinned, back-illuminated, high-resolution (1024 X 1024; 24 μm pixels) CCD imaging chip with an anti-reflective (UVAR) coating on its active area to improve its sensitivity to light from the scintillator. The chip is cryogenically cooled with LN_2 and operated at a controller-stabilized temperature of -120 °C which effectively eliminates thermal electronic noise buildup in the pixel wells (the typical dark current is $\lesssim$ 1 electron/pixel/hr). This allows for extended image integration times ($\approx$ 1 hr) and greatly enhances the sensitivity of the camera in low light situations; however, it also requires that the shutter housing on the camera assembly be continuously purged with dry nitrogen gas to minimize the risk of vapor condensation on the CCD vacuum-barrier window. Data is downloaded to the camera controller using a 16-bit A/D converter running at 50 kHz which imposes an average read-out noise on the image of $\approx$ 5 electrons/pixel. When compared to the full well capacity of the CCD chip ($\approx$ 325,000 electrons/pixel), this implies an effective dynamic range for the camera in excess of $\approx$ 50,000 (a broad dynamic range is essential in tomographic imaging problems involving thick objects since the camera must be able to resolve subtle intensity variations in the "shadowed" portion of an image without saturating in adjacent "open field" segments). A thin (0.125"), front-surfaced mirror fabricated from aluminized Pyrex glass is used to reflect light from the scintillator through an angle of 90° into the camera assembly which is mounted on dual-axis optical rails adjacent to (but well out of) the direct neutron beam path (the scintillator-to-CCD distance is $\approx$ 65 cm). The entire detector assembly is housed in a light-tight plywood enclosure with thin (0.125") aluminum entrance and exit apertures for the neutron beam (*cf.* Figure 1).

Two similar scintillator materials have been tested in the prototype imaging detector thus far, BC-400 and BC-408, and both worked well[b]. These materials are rigid, transparent, polyvinyltoluene-based plastics with H/C ratios $\approx$ 1.1:1, refractive indices $\approx$ 1.58 and relatively narrow, single-band emission spectra that peak near $\approx$ 425 nm which make them a reasonably good (though not ideal) match to the quantum efficiency curve of the CCD camera chip. Both have high light outputs for neutrons in the 10 – 15 MeV energy range ($\approx$ 29,000 photons per interacting neutron), low relative sensitivities to incident gammas (*e.g.* $S_\gamma(\text{erg}/\gamma\text{-MeV})/S_n(\text{erg/n}) \approx 0.30$ for incident 14 MeV neutrons)[26,27] and fast luminescent decay times ($\approx$ 2.5 ns). The scintillators used in the experiments presented here were cut as rectangular slabs (30 cm X 30 cm) with a thickness of 4 cm (the limited focal depth of the fast lens on the camera effectively restricts the scintillator thickness to $\lesssim$ 5 cm due to the close-in imaging geometry used here). The mean free path for (n,p) reactions responsible for generating light in the scintillators ranges from 20.17 cm at 10 MeV to 29.47 cm at 15 MeV. This implies neutron detection efficiencies (ε) of $\approx$ 12.8% - 18.0% for a 4-cm scintillator over the energy range of interest.

The relatively high resolving power of the CCD imaging chip ($\approx$ 20 lp/mm) and modest image reduction factor used in the prototype detector (image-to-chip size ratio $\approx$ 0.091) imply that the ultimate spatial resolution of the imaging detector is essentially limited by the apparent size of the light pulse generated by the recoiling proton ejected when a neutron interacts in the scintillator. For plastics analogous to those used here, nuclear kinematic calculations and detailed Monte Carlo scattering simulations predict an apparent pulse size of $\approx$ 0.70 mm (FWHM) for neutrons interacting along the centerline of the scintillator[28-30] (this, of course, must be folded with the spot size of the neutron source and the overall imaging system magnification factor to determine the actual spatial resolution at the object position). Theoretical modulation transfer function (MTF) curves calculated for the various imaging system components (*cf.* Figure 2) predict an ultimate spatial resolution at the object position (*i.e.* lp/mm as MTF -> 0) of $\approx$ 2.80 lp/mm for the detector considered alone and $\approx$ 1.90 lp/mm for the system as a whole (this assumes an image magnification factor of $\approx$ 2:1 and a source spot size of $\approx$ 1.25 mm).

2.2 Multi-axis staging system

The multi-axis staging system used to support and manipulate objects during testing of the prototype imaging detector was designed and built by personnel assigned to support this project at the Westinghouse Savannah River Company (WSRC) in Aiken, SC.[31] The system consists of a high-precision (digital) rotation table mounted on a translation stage with two degrees of freedom ($\pm$ y and $\pm$ z perpendicular to beam axis). The overall assembly has a load capacity in excess of $\approx$ 200 lbs.

---

[b] BC-400 and BC-408 are trade names for rigid, transparent plastic scintillator materials manufactured by the BICRON Corporation, 12345 Kinsman Road, Newbury, OH 44065-9577.

and can be operated remotely from a control room area. The stage controller is driven by an IBM PC clone running a custom LabVIEW[c] program developed by WSRC which links the movements of the stage to the IPLab Spectrum[d] image acquisition software running on an adjacent Macintosh G3 computer. The LabVIEW program is sufficiently powerful to allow for fully-automated (unattended) operation of the entire system. The program continuously monitors and records the neutron flux incident on the test object, signals the CCD camera to initiate image acquisition for a prescribed time (or waits if sufficient neutron flux is not detected at the object position), instructs IPLab Spectrum to store valid images on the Macintosh hard disk at the end of a run (or repeat images if the integrated neutron flux fails to exceed a given threshold) and then resets the camera before beginning the next imaging cycle. During extended tomographic imaging runs, the program also drives the rotation table to turn the object under inspection through a prescribed set of angular positions spanning 180°. This is normally done in a series of one-way passes around the object with each pass uniformly splitting the range of angles imaged during the previous pass (this allows us to recover a complete, evenly-distributed tomographic data set after each pass even if the imaging system fails for some reason during the run sequence).

3. RECENT IMAGING EXPERIMENTS

3.1 Experimental setup

The Ohio University Accelerator Laboratory (OUAL) in Athens, OH has been chosen as a test bed for evaluating the performance of the prototype imaging detector and multi-axis staging system. The OUAL facility features a physical layout which is generally similar (albeit on a somewhat larger scale) to that which we have proposed for an actual neutron imaging facility and the OUAL technical staff has a wealth of experience in the production of intense, accelerator-driven, high-energy neutron beams for research purposes.

In the imaging experiments described here, a nearly monoenergetic 10-MeV neutron beam was generated by focussing 6.85-MeV D^+ ions extracted from the OUAL tandem van de Graaff accelerator into a cylindrical, 1-cm-diameter, 8-cm-long D_2 gas cell attached to the end of a beam line. The gas cell was capped with thin ($\approx$ 5 μm) W entrance and exit windows and maintained at a static pressure of $\approx$ 40 psia ($\approx$ 2.7 atm) which limited the spread in energy of the resulting $D(d,n)^3He$ neutrons to $\lesssim$ 500 keV. Typical D^+ ion currents measured at the gas cell were $\approx$ 7.5 μA during the runs and the diameter of the beam focal spot at the entrance window to the cell was $\lesssim$ 3 mm. This resulted in an equivalent neutron yield $\approx 5\times10^{10}/4\pi$ n/sec/sr along the beam axis (*i.e.* $\approx$ 1/20th of the intensity required for the source in our proposed imaging system but still sufficient to evaluate the performance of the prototype detector).

The test objects imaged in the experiments were mounted on the multi-axis staging system which was located on the beam axis $\approx$ 2 m downstream from the neutron source (no shielding or neutron collimation was used between the source and stage). The prototype imaging detector was located in a shielded detector cave $\approx$ 2 m further downstream behind a thick ($\approx$ 1.5 m) concrete and steel wall with a tapered polyethylene collimator. This provided a 2:1 image magnification factor with a clear field-of-view (FOV) $\approx$ 12" in diameter at the detector position ($\Rightarrow$ FOV diameter $\approx$ 6" at the object position). While essentially a mater of convenience in these experiments, our Monte Carlo simulations of a variety of possible imaging configurations indicate that a 2:1 image magnification factor also serves to minimize radiation backgrounds at the scintillator associated with "internal" scattering within the object under inspection (internal scattering can present a problem when imaging thick objects with curved contours since particles scattered near the limb suffer very little attenuation in the object and can therefore make a potentially significant contribution to the radiation background at the imaging plane). The full-scale imaging system that we propose will also have a 2:1 image magnification factor but may have a somewhat larger first conjugate (source-to-object) distance than the 2 m spacing used here.

3.2 Imaging results

Four series of imaging experiments have thus far been carried out at OUAL (10/97, 01/98, 12/98 and 05/99). The first included radiographic (single view) imaging of a 5"-thick Pb and polyethylene slab assembly (with features machined into the poly) and a set of nine conventional step wedges. Radiation background levels at the detector position were also measured during this run by attaching a standard laboratory TLD monitor to the shutter housing on the CCD camera. The second series included radiographic imaging of a 3"-thick depleted uranium (D-38) and lithium deuteride slab assembly (similar in design

---

[c] LabVIEW is the trade name for a graphical programming software package marketed by National Instruments Corporation, 11500 N. Mopac Expressway, Austin, TX 78759-3504.

[d] IPLab Spectrum is the trade name for an image acquisition and analysis software package marketed by Scanalytic, Inc., 8550 Lee Highway, Suite 400, Fairfax, VA 22031-1515.

to the Pb/poly assembly imaged earlier) and tomographic (multiple view) imaging of a 4"-OD, 2"-ID Pb cylinder with a polyethylene core (again with features machined into the poly). Edge resolution measurements were also done during this run by imaging the machined surface of a 2.3"-thick Cu block optically aligned with the beam axis. The third series included radiographic imaging of a 6"-thick D-38 and polyethylene slab assembly (with features machined into both the D-38 and the poly). The fourth series of experiments (still being analyzed) included tomographic imaging of a 4"-OD, 1.5"-ID HeviMet (WniFe) cylinder with a 0.125"-wall brass sleeve insert and a polyethylene core (the brass sleeve and poly core were each cut slightly undersized to allow for tilting and/or offsetting of the pieces within the HeviMet shell and each had a variety of features machined into it to test system performance). A thin (2.4 mm) sample of a new type of ZnS(Ag)-doped polypropylene scintillator was also tested during this run as a possible alternative to our present BC-400 and BC-408 plastic scintillators. Due to space restrictions, only selected results from these imaging experiments will be presented in this work (the full data set is available from the principal author upon request).

The step wedges imaged during the first series of experiments were fabricated from Pb, lucite, mock high explosive, Al, Be, graphite, brass, polyethylene, and stainless steel. All were 0.5"-thick pieces with uniform steps ranging from 0.5" to 5.0" in width. The areal densities (ρx) of the steps ranged from 1.21 g/cm^2 (0.50" step in poly wedge) to 144.78 g/cm^2 (5.00" step in Pb wedge). The nine different wedges were grouped together and radiographed as a single unit (looking "up the steps") in a series of two 1 hr exposures (time integrated flux at object position $\approx 3.6\text{x}10^8$ n/cm^2) with each generating $\approx$ 125 - 475 counts/pixel above the CCD camera's built-in DC offset level of $\approx$ 90 counts/pixel. All of steps in each of the materials within in the detector FOV are discernable in the final processed image (*cf.* Figure 3).

Background radiation levels at the detector position were also measured during this run to assess shielding requirements. This was done by attaching a standard laboratory TLD monitor to the shutter housing on the CCD camera. The total gamma and neutron dose rates (integrated over several hours) were found to be $\lesssim$ 10 mrem/hr and $\lesssim$ 20 mrem/hr, respectively. These levels are not considered problematic.

The Pb cylinder used for tomographic imaging tests during the second series of experiments at OUAL had an OD of 4" and an ID of 2" with a polyethylene core. The poly core was split into two half-cylinders with one serving as a "blank" and the other having a series of 10-, 8-, 6-, 4-, and 2-mm-diameter, 0.5"-deep holes machined into its outer (curved) surface (*cf.* Figure 4). The areal density of the assembly ranged from 62.38 g/cm^2 (along the centerline) to 99.69 g/cm^2 (along the limb of the core). A series of 64 10 min exposures (time integrated flux at object position $\approx 3.8\text{x}10^9$ n/cm^2) were taken of the assembly at angles evenly distributed over 180° with each generating $\approx$ 300 – 500 counts/pixel above the camera's DC offset level. Tomographic reconstructions of the object done for 1-mm-thick slices taken through each of the holes in the poly core (perpendicular to the cylinder axis) clearly show the core's structure (*cf.* Figure 5). Note that, although not well resolved, the narrow ($\lesssim$ 0.010") gap between the two halves of the poly core is also visible in the reconstructed images.

TheD-38/poly slab assembly imaged during the third series of experiments is the thickest object imaged thus far in our testing of the prototype detector. It consisted of two adjacent 4" X 4" X 1"-thick polyethylene slabs shielded by up to 4" of depleted uranium. The first poly slab had two series of 10-, 8-, 6-, 4- and 2-mm-diameter, flat-bottomed holes machined to depths of 0.5" (half-thickness) and 1" (full thickness) and two additional 2-mm-diameter holes machined to depths of 0.250" and 0.125" (the latter corresponds to a volume defect of $\approx$ 10 mm^3 and an areal density defect of $\approx$ 0.30 g/cm^2). The second poly slab was a blank used to increase the overall object thickness. One of the D-38 plates used for shielding was cut into two stacked pieces (to produce a contact gap) and had a series of 4-mm-diameter, flat-bottomed holes machined to depths ranging from 0.5" to 0.010" (an areal density defect of $\approx$ 0.50 g/cm^2). The areal densities of the various configurations imaged ranged from 4.83 g/cm^2 (bare poly slabs) to 197.36 g/cm^2 (fully shielded slabs). A series of 45 30-minute exposures (time integrated flux at object position $\approx 8.1\text{x}10^9$ n/cm^2) were taken of the poly slabs shielded by 2" of D-38 with each generating $\approx$ 555 - 665 counts/pixel above the camera's DC offset level. The final processed image and associated lineouts (*cf.* Figure 6) clearly show the detailed structure of the poly slab and the machined D-38 plate. The fully-shielded assembly was imaged in another series of 176 30 min exposures (time integrated flux at object position $\approx 3.2\text{x}10^{10}$ n/cm^2) with each generating $\approx$ 315 - 335 counts/pixel above the DC offset level. The final processed image and associated lineouts (*cf.* Figure 7) again show the full structure of the poly slab (including even the smallest, 2-mm-diameter, 0.125"-deep hole) and features as small as a 4-mm-diameter, 0.020"-deep hole in the machined D-38 plate.

3.3 Notes on image processing

The raw images taken during both series of experiments at OUAL initially bore random distributions of sharp "spikes" rising from several hundred to several thousand counts above the local background. The number of pixels affected varied in

direct proportion to the image integration time but rarely exceeded ≈ 10% of the total. The spikes were determined to be due to a combination of cosmic-ray strikes and (n,α) reactions in the silicon-based CCD chip. They were usually well-separated from one another and occupied only one or two pixels in any given neighborhood within the image. These anomalies were surgically removed during online post-processing of the images at OUAL using an adaptive algorithm that we developed which first identifies and then corrects pixels that deviate from the mean value of their (statistically valid) nearest neighbors by more than a prescribed amount (*cf.* Figure 8). Statistically valid pixels in the image are not altered in any way using our algorithm (unlike conventional "smoothing" or Fast Fourier Transform (FFT) algorithms) and image details larger than ≈ 3 X 3 pixels (≈ 0.50 mm at the object position in the case of these experiments) are preserved. The raw images also exhibited an axially-symmetric roll-off in intensity toward their outer edges. This effect is characteristic of fast camera lenses such as ours operated at close quarters and was factored out by dividing each image by a normalized "open field" image to obtain the final forms presented here.

Tomographic reconstruction of the Pb/poly cylinder data was done offline using a "Constrained Conjugate Gradient" (CCG) algorithm developed by D. Goodman at LLNL[32] with non-negativity of voxel densities as the only constraint. The CCG algorithm provides a significant advantage in the tomographic imaging of thick objects such as this since it tends to produce much cleaner reconstructed images than conventional Filtered Back-Projection (FBP) algorithms (*cf.* Figure 9).

Finally, we should note that, while every effort has been made to produce prints of the highest possible quality for publication here, it is extremely difficult to reproduce the level of detail that high-resolution, "on-screen" renderings of the images provide. Our comments on the clarity of the images obtained during the experiments at OUAL are based entirely on computer-graphic representations and lineouts through relevant parts of the images.

4. NEUTRON SOURCE DEVELOPMENT

The development of an intense, high-energy neutron source suitable for use in a full-scale imaging system is proceeding in parallel with our work on the prototype detector and staging system. As noted above, we propose to use an accelerator-driven $D(d,n)^3He$ neutron source operating in the 10 - 15 MeV energy range. In order to meet our performance goals, the source will need to have an equivalent neutron yield ≈ $10^{12}/4\pi$ n/sec/sr along the beam axis and an effective focal spot size ≈ 1 – 1.5 mm (FWHM). A high-energy DD neutron source is preferred here over a more conventional DT source because it provides natural, kinematic collimation of the neutron beam (which minimizes "external" scattering from walls, floors, etc. and thereby reduces radiation shielding requirements) and offers the potential for an effectively indefinite operational lifetime without posing the problems typically associated with handling tritium targets. We are working with vendors to establish the existence of small accelerator systems suitable for use in a full-scale neutron imaging system. The most promising systems appear to be either a compact radio-frequency quadruplole (RFQ) accelerator coupled to a drift-tube linac (DTL) or a small cyclotron. In either case, the accelerator system will have to deliver an average D^+ ion current ≈ 200 - 250 μA at the gas cell in order to produce a neutron flux sufficient to image objects of interest. While this is certainly achievable with current technology, it does pose another, in some ways more challenging, problem: the combined requirements of a high D^+ ion current and small focal spot size effectively preclude the use of conventional ("windowed") D_2 gas cell designs due to their general inability to handle the immense heat loads involved. A more innovative approach is required.

We are currently collaborating with R. Lanza at the Massachusetts Institute of Technology (MIT) on the development of a "windowless" D_2 gas target assembly which can be coupled to a high-current, pulsed accelerator. The target design was first implemented by E. Iverson at MIT[33] and subsequently perfected by K. Richardson and J. Guzek, *et al.* at a South African laboratory[34]. The target will consist of a high-pressure (≈ 2 - 3 atm) D_2 gas cell mounted at the exit port of a differentially-pumped chamber with three stages isolated from one another by a series of rotating disks with apertures synchronized to the pulse frequency of the accelerator (*cf.* Figure 10a). A windowless target assembly such as this will minimize energy loss in the deuterium beam and is particularly well suited to use with small accelerator systems such as RFQ linacs which tend to operate with very high peak ion currents and relatively low duty factors. Operational testing of a prototype system is currently underway at MIT.[35]

An alternative to the "rotating aperture" target design is also being pursued at MIT. The basic technique, first proposed by A. Hershcovitch of Brookhaven National Laboratory (BNL),[36-38] involves the use of an intense, axial plasma discharge to effectively "plug" the aperture of a high-pressure gas cell by rapidly heating and ionizing gas leaking down the exit channel. This increases the viscosity of the gas in the channel and creates a region with high pressure but low density which can balance the pressure in the cell and yet remain relatively transparent to a charged particle beam. In recent tests of a prototype target at MIT using an Ar gas cell, W. Gerber and A. Hershcovitch, *et al.* have reported the ability to sustain pressure differ-

entials of more than 2.5 atm across a small (≈ 3 mm) aperture with an upstream pressure of ≈ 10^{-6} torr.[39] This approach offers several advantages over the "rotating aperture" design. First (and most obvious), it has no moving parts and is thus easier to assemble and maintain. Second, it operates in a "steady-state" mode which allows for the use of CW beams and greatly reduces the thermodynamic stress on the gas in the cell. Finally, it has a favorable focusing effect on charged particle beams. The main drawback to this design is that it has relatively complicated cooling requirements which could affect its reliability. We are currently working with MIT to design and test a high-pressure "plasma window" D_2 gas cell to assess its potential as a target for use in our imaging system (*cf.* Figure 10b).

5. CONCLUSIONS

The experiments described here have demonstrated the essential feasibility of using high-energy neutron imaging as a thick-target inspection tool and we are now poised to commit to the construction of a full-scale facility. Additional tests of the prototype imaging detector are planned at OUAL (focussed primarily on improving the light collection efficiency of the system and evaluating alternate scintillator materials) and key decisions on target ("rotating window" vs. "plasma window") and accelerator (RFQ/DTL vs. cyclotron) technologies will be made early next year.

ACKNOWLEDGMENTS

We would like to thank Marc Loibl, Vito Casella, Mark Goodell, David Immel, Rick Poland and Wayne Young of WSRC for their outstanding support in developing and maintaining the multi-axis staging system used in these experiments and (especially) for automating the image acquisition process. We would also like to thank Profs. David Ingram and Roger Finlay of Ohio University and the staff of OUAL for their continued support in the testing of our prototype imaging detector and Dr. Harry Martz of LLNL for his help in doing tomographic image reconstructions. Finally, we would like to thank Prof. Richard Lanza of MIT and his student, William Gerber, for their support in the ongoing development of the high-yield neutron source.

This work was performed at the University of California, Lawrence Livermore National Laboratory, under the auspices of the U.S. Department of Energy (contract # W-7405-Eng-48).

REFERENCES

1. C. Fischer, J. Stade and W. Bock (eds.), *Proceedings of the Fifth World Conference on Neutron Radiography*, Berlin, Germany (June 17–20, 1996): Deutsche Gesellschaft für Zerstörungsfreie Prüfung E.V. (DGZfP), 1997, 769 pp.; see also published proceedings of previous conferences in this series.
2. G. Imel and G. McClellan, "Survey of neutron radiography facilities," published in C. Fischer, *et al.* (ref. 1), p. 524-531.
3. E. Criscuolo and D. Polansky, "Fast neutron radiography," published in *Proceedings of the Missiles and Rockets Symposium*, U.S. Naval Ammunition Depot, Concord, CA, 1961, p. 112-115.
4. D. Polansky and E. Criscuolo, "Radiographic aspects of fast neutron detection," published in *Proceedings of the 24th National Conference of the American Society for Nondestructive Testing*, Philadelphia, PA, 1964.
5. J, Anderson, S. Osborn and R. Tomlinson, "Neutron radiography in man," British Journal of Radiology, **37**, p. 957–958 (1964).
6. E. Tochilin, "Photographic detection of fast neutrons: application to neutron radiography," Physics in Medicine and Biology, **10**, p. 477–490 (1965).
7. D. Wood, "Fast neutron radiography with a neutron generator," Transaction of the American Nuclear Society, **10**, p. 443–444 (1967).
8. P. Parks, M. Brown, D. Harmer, "Problems of fast neutron radiography," Biomedical Sciences Instrumentation, **6**, p. 118–126 (1969).
9. H. Berger, "Some experiments in fast neutron radiography," Materials Evaluation, **27**, p. 245–253 (1969).
10. H. Berger, "Image detection methods for 14.5 MeV neutrons: techniques and applications," International Journal of Applied Radiation and Isotopes, **21**, p. 59–70 (1970).
11. A. Richardson, "Improved images in 14.5 MeV neutron radiography," Materials Evaluation, **35**, p. 52–58 (1977).
12. E Bagge, E Dühmke, W. Enge, W. Hunger, U. Roose and R. Scherzer, "Fast neutron radiography for extended objects by a plastic detector technique," Nuclear Instruments and Methods, **147**, p. 109–114 (1977).
13. J. Brzosko, B. Robouch, L. Ingrosso, A. Bortolotti and V. Nardi, "Advantages and limits of 14-MeV neutron radiography," Nuclear Instruments and Methods in Physics Research, **B72**, p. 119–131 (1992).
14. R. Klann, Argonne National Laboratory, P.O. Box 2528, Idaho Falls, ID 83403, "A system for fast neutron radiography", 5 pp., unpublished manuscript obtained from author (1996).

15. A. Gavron, K. Morley, C. Morris, S. Seestrom, J. Ullmann, G. Yeats and J. Zumbro, "High-energy neutron radiography," published in G. Vourvopoulos (ed.), *Proceedings of the International Conference on Neutrons in Research and Industry* (SPIE **2867**), Crete, Greece (June 9-15, 1996): SPIE Press, 1997, p. 326-331.
16. C. Morris, V. Armijo, L. Atencio, A. Bridge, A. Gavron, G. Hart, K. Morley, T. Mottershead, G. Yeats and J. Zumbro, "An integrating image detector for high energy neutrons," published in G. Vourvopoulos (ref. 15), p. 351-357.
17. J. Watterson, J. Guzek, U. Tapper and S. Surujhal, "The development of a computational model for fast neutron radiography," published in G. Vourvopoulos (ref. 15), p. 358-361.
18. R. Klann and M. Natale, "Fast neutron radiography research at ANL-W," published in C. Fischer, *et al.* (ref. 1), p. 382-390.
19. R. Klann, "Fast neutron (14.5 MeV) radiography: a comparative study," published in C. Fischer, *et al.* (ref. 1), p. 469-483.
20. R. Ambrosi and J. Watterson, "Factors affecting image formation in accelerator-based fast neutron radiography," Nuclear Instruments and Methods in Physics Research, **B139**, p. 279–285 (1998).
21. R. Ambrosi, J. Watterson and B. Kala, "A Monte Carlo study of the effect of neutron scattering in a fast neutron radiography facility," Nuclear Instruments and Methods in Physics Research, **B139**, p. 286–292 (1998).
22. H. Rahmanian and J. Watterson, "Optimisation of light output from zinc sulfide scintillators for fast neutron radiography," Nuclear Instruments and Methods in Physics Research, **B139**, p. 466–470 (1998).
23. F. Dietrich and J. Hall, "Detector concept for neutron tomography in the 10 - 15 MeV energy range", LLNL report # UCRL-ID-123490, 4 pp. (1996).
24. F. Dietrich, J. Hall and C. Logan, "Conceptual design for a neutron imaging system for thick target analysis operating in the 10 - 15 MeV energy range," published in J. Duggan and I. Morgan (eds.), *Application of Accelerators in Research and Industry* (AIP **CP392**), New York, NY: AIP Press, 1997, p. 837-840.
25. T. Sammons, *EL PINEX Handbook,* EG&G training manual # 1183-4229, 245 pp. (1982).
26. D. Clark and E. Lent, "The neutron and gamma sensitivities of plastic scintillators," LLNL memo # UOPAD-75-20, 27 pp. (1975).
27. H. Koehler, J. Kammeraad, B. Davis and E. Burns, "PINEX fluor characteristics," LLNL memo # DDG-88-29, 21 pp. (1988).
28. T. Perry, "Resolution of neutrons [in plastic scintillators]," LLNL memo # UOPE-75-102, 10 pp. (1975).
29. D. Goosman, "Calculations of the transverse spatial distribution of NE-102 scintillation light made by recoil protons from collimated 14 MeV neutrons," LLNL report # UCRL-52651, 6 pp. (1979).
30. B. Jacoby, "Impulse response of neutrons and gammas for fluors," LLNL memo # DDG-88-29, 10 pp. (1991).
31. V. Casella, M. Goodell, D. Immel, R. Poland and W. Young, "Design and implementation of an automated target staging system for neutron radiographic computer tomography imaging," presented at the ASNT 1998 Fall Conference, Nashville, TN, October 19–23, 1998.
32. D. Goodman, E. Johansson and T. Lawrence, "On applying the conjugate gradient algorithm to image processing problems," published in C. Rao (ed.), *Multivariate Analysis: Future Directions*, Oxford, U.K.: Elsevier Science Publishers, 1993, p. 209-232; also H. Martz, LLNL, P.O. Box 808, M/S L-333, Livermore, CA 94550 (private communication).
33. E. Iverson, "Windowless gas target for neutron production," Ph.D. thesis under R. Lanza and L. Lidsky, Massachusetts Institute of Technology, 154 pp. (February 1997).
34. K. Richardson, J. Guzek, A. Waites, C. Franklyn, W. McMurray, J, Watterson and U. Tapper, "The design of a differentially-pumped gas target system for the generation of intense monoenergetic fast neutron beams," preprint of paper submitted for publication; also J. Guzek, Schonland Research Centre, University of Witwatersrand, Johannesburg, 2050, South Africa (private communication).
35. W. Gerber, "Investigation of windowless gas target systems for particle accelerators," M.S. thesis under R. Lanza and L. Lidsky, Massachusetts Institute of Technology, 77 pp. (June 1998).
36. A. Hershcovitch, "High-pressure arcs as vacuum-atmosphere interface and plasma lens for non-vacuum electron beam welding machines, electron beam melting and non-vacuum ion material modification," Journal of Applied Physics **78** (9), 5283-5288 (1995).
37. A. Hershcovitch, "A plasma window for vacuum-atmosphere interface and focusing lens of sources for non-vacuum ion material modification," Review of Scientific Instruments **69** (2), 868-873 (1998).
38. A. Hershcovitch, "A plasma window for transmission of particle beams and radiation from vacuum to atmosphere for various applications," Physics of Plasmas **5** (5), 2130-2136 (1998).
39. W. Gerber, R. Lanza, A. Hershcovitch, P. Stephan, C. Castle and E. Johnson, "The plasma porthole: a windowless vacuum-pressure interface with various accelerator applications," presented at the 15th International Conference on the Application of Accelerators in Research and Industry (CAARI'98), Denton, TX, November 4–7, 1998.

COLLECTED FIGURES

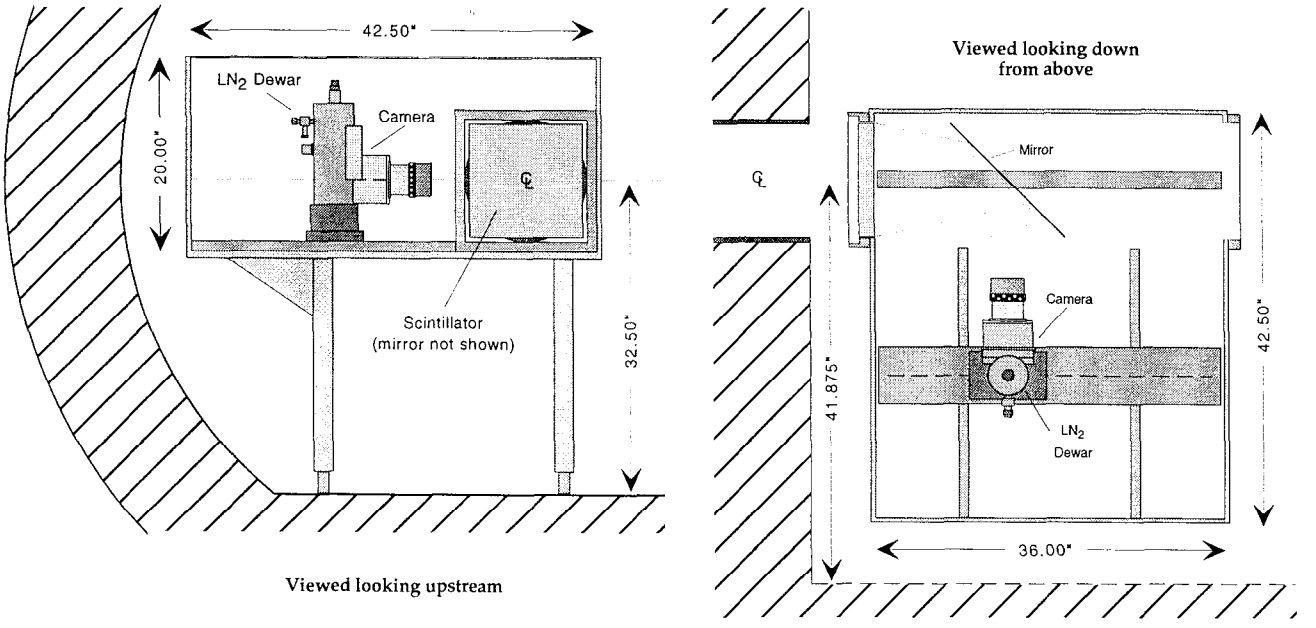

Figure 1. Generalized schematic of prototype imaging detector (plastic scintillator, turning mirror and LN2-cooled CCD camera assembly) housed in light-tight enclosure.

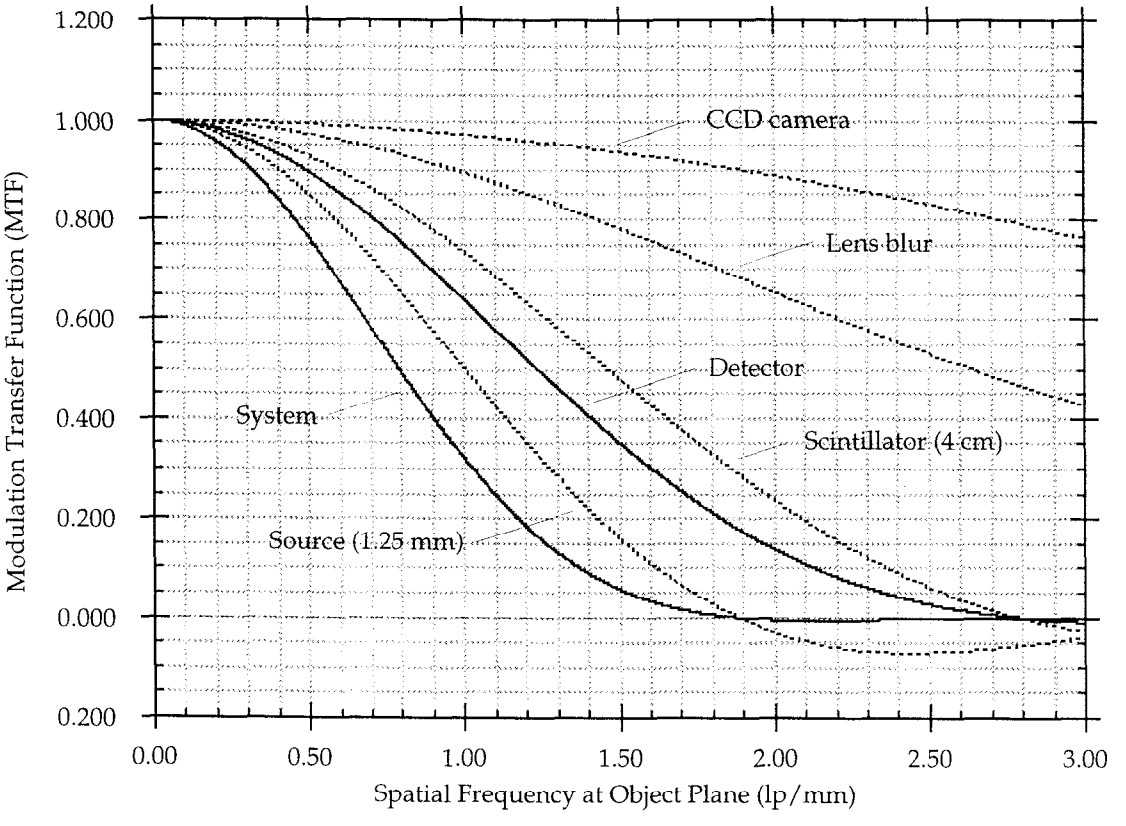

Figure 2. Modulation Transfer Function (MTF) curves for imaging system components projected to object position (assumes 2:1 image magnification factor and source spot size ≈ 1.25 mm).

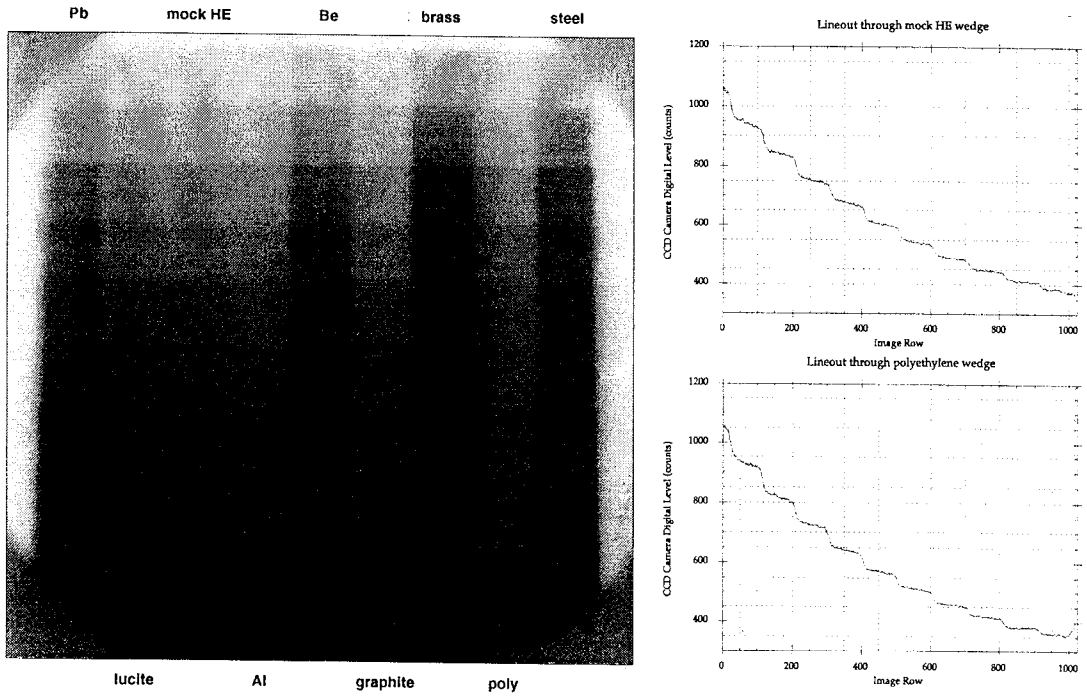

Figure 3. Final processed image of grouped step wedges (looking left to right, the materials are Pb, lucite, mock high explosive, Al, Be, graphite, brass, polyethylene, and stainless steel).

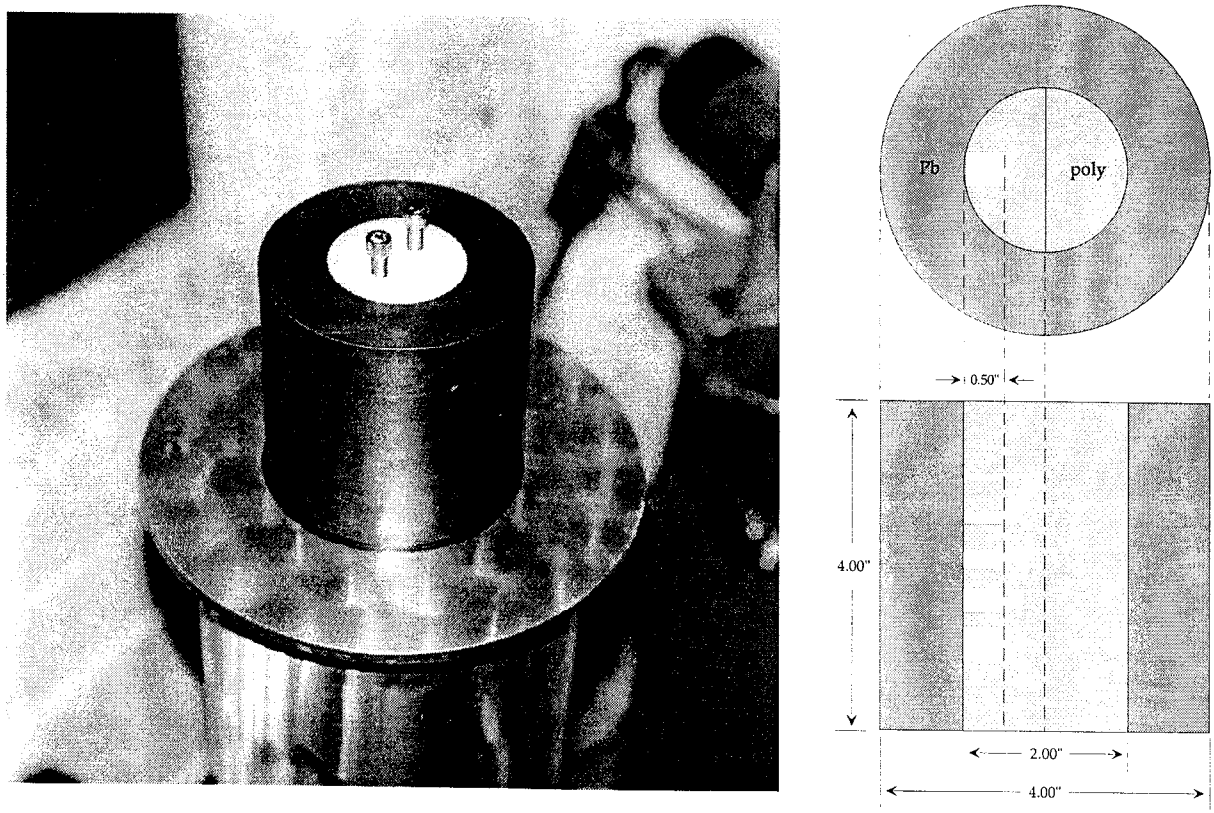

Figure 4. Right-circular Pb cylinder with polyethylene insert used for tomographic imaging tests. The insert was split into two half-cylinders with one serving as a "blank" and the other having a series of holes machined into its outer (curved) surface.

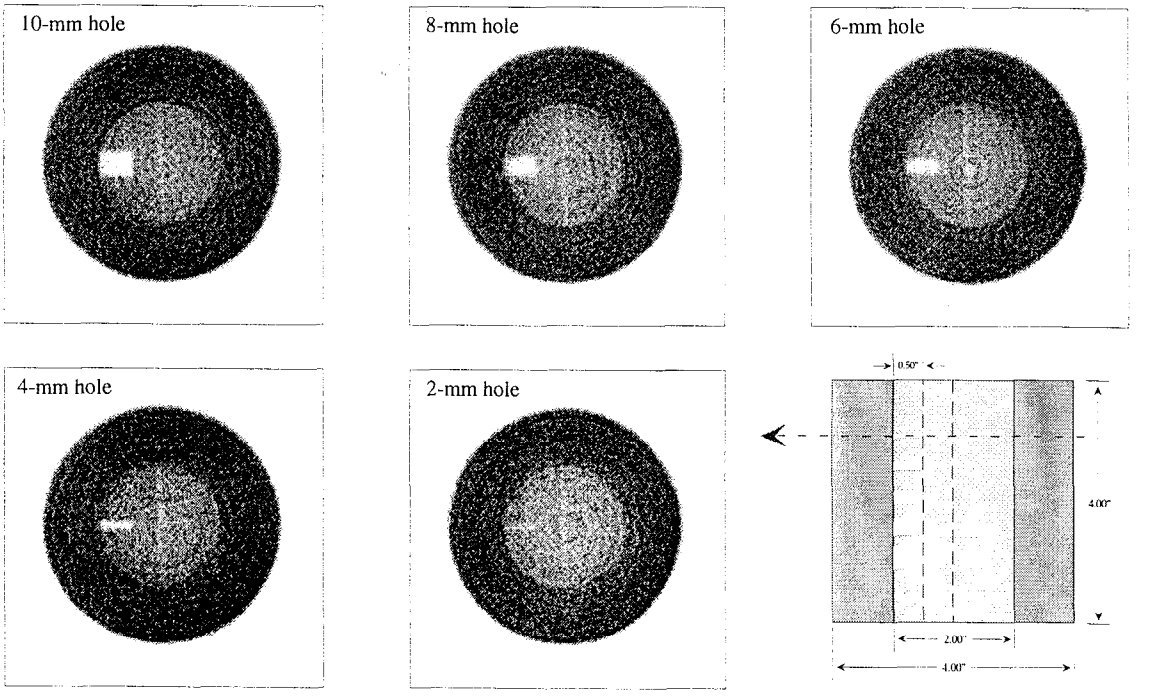

Figure 5. Tomographic reconstructions of cylindrical Pb and polyethylene test object done for 1-mm-thick slices taken through holes in poly core (perpendicular to cylinder axis). Notc narrow gap between the two halves of poly core.

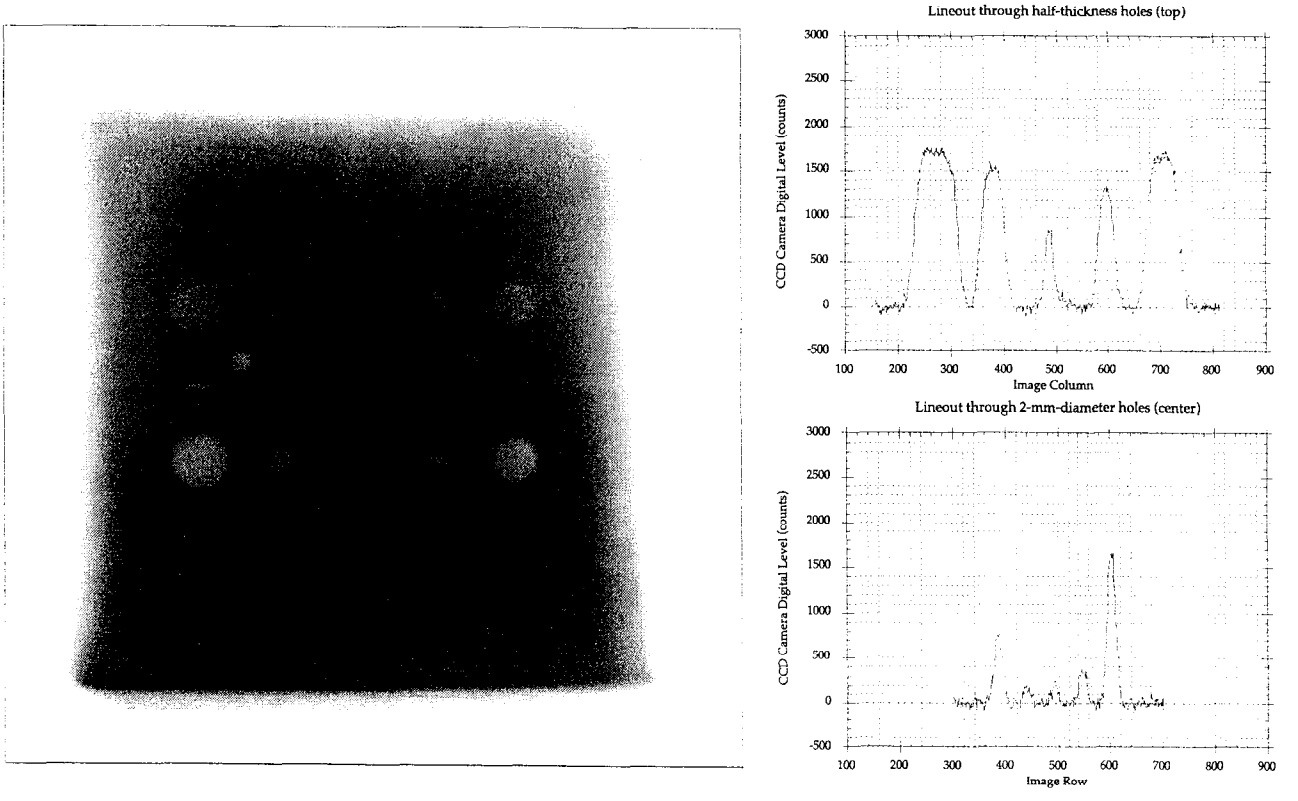

Figure 6. Final processed image of polyethylene slabs shielded by 2" of depleted uranium. (D-38) The image and associated lineouts clearly show the detailed structure of the poly slab and the machined D-38 plate.

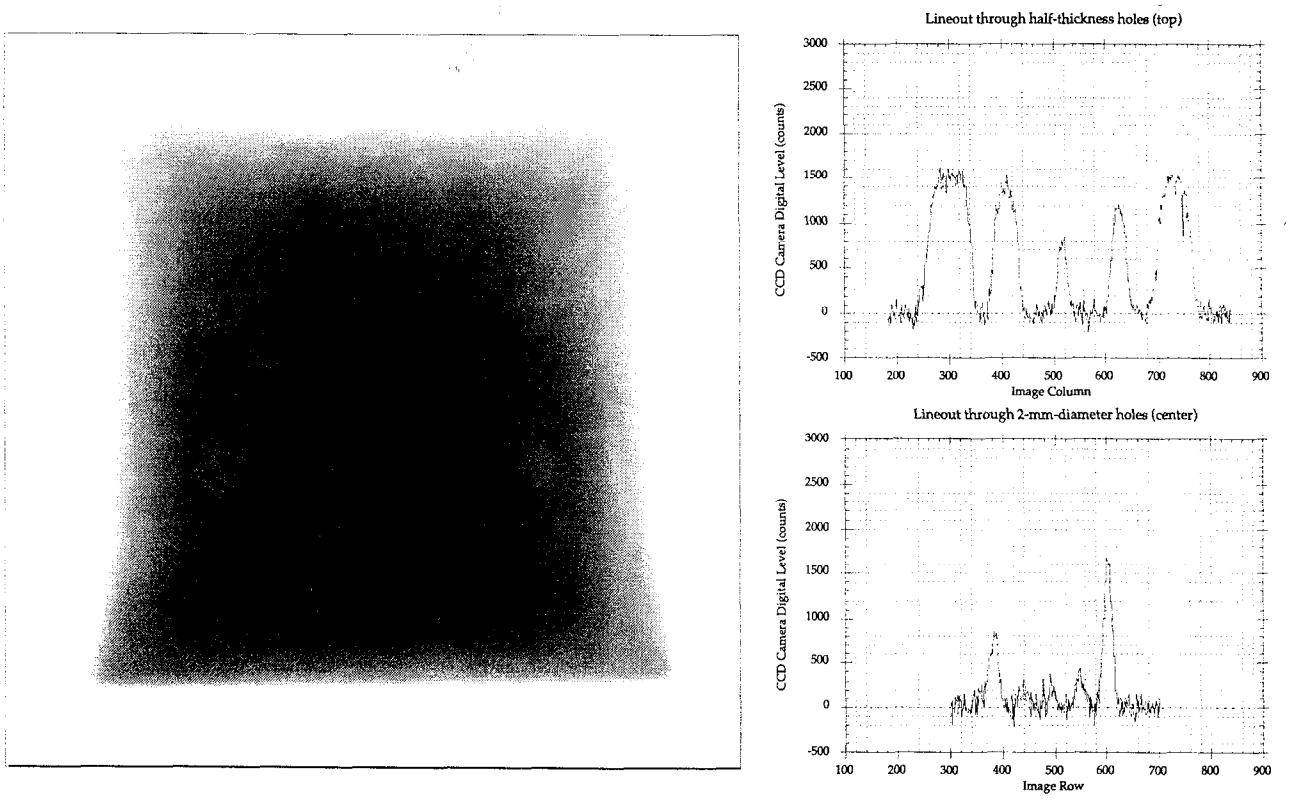

Figure 7. Final processed image of fully-shielded D-38/poly assembly (2" of poly shielded by 4" of D-38). The image and associated line-outs again show the full structure of the poly slab and most features in the machined D-38 plate.

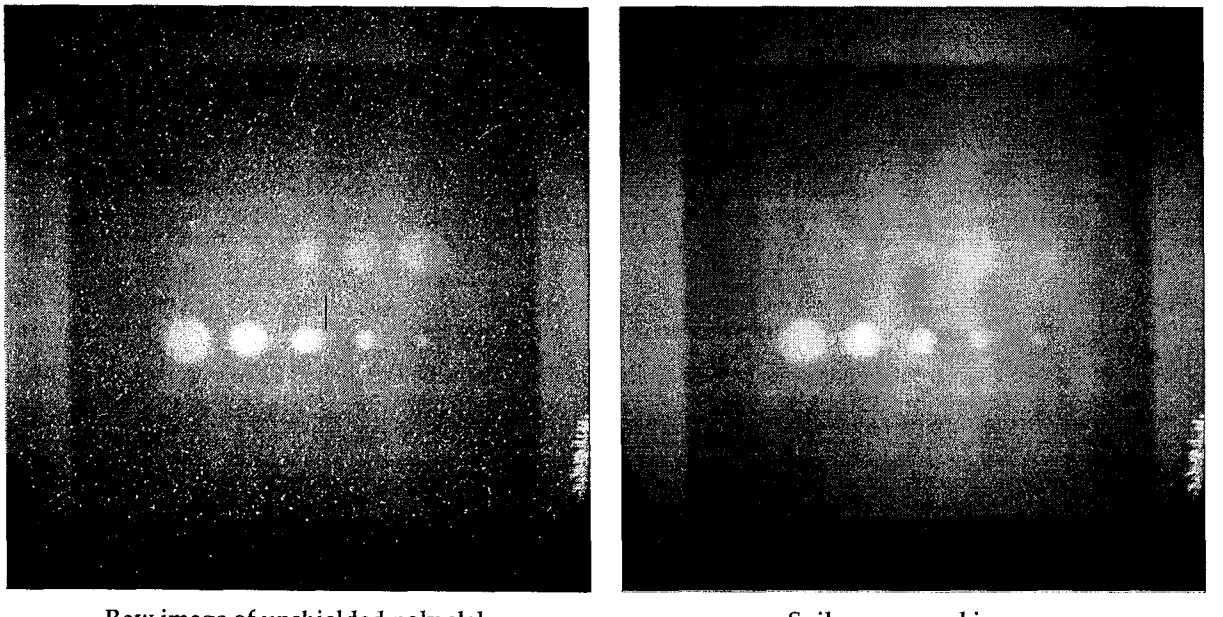

Raw image of unshielded poly slab (1 hr exposure)

Spike-processed image (not corrected for roll-off)

Figure 8. Raw image of unshielded polyethylene slab (1 hr exposure) compared to "spike-processed" image (not corrected for roll-off). The processing algorithm identifies and corrects pixels that deviate from the mean value of their nearest neighbors by more than a prescribed amount (leaving statistically valid pixels unchanged).

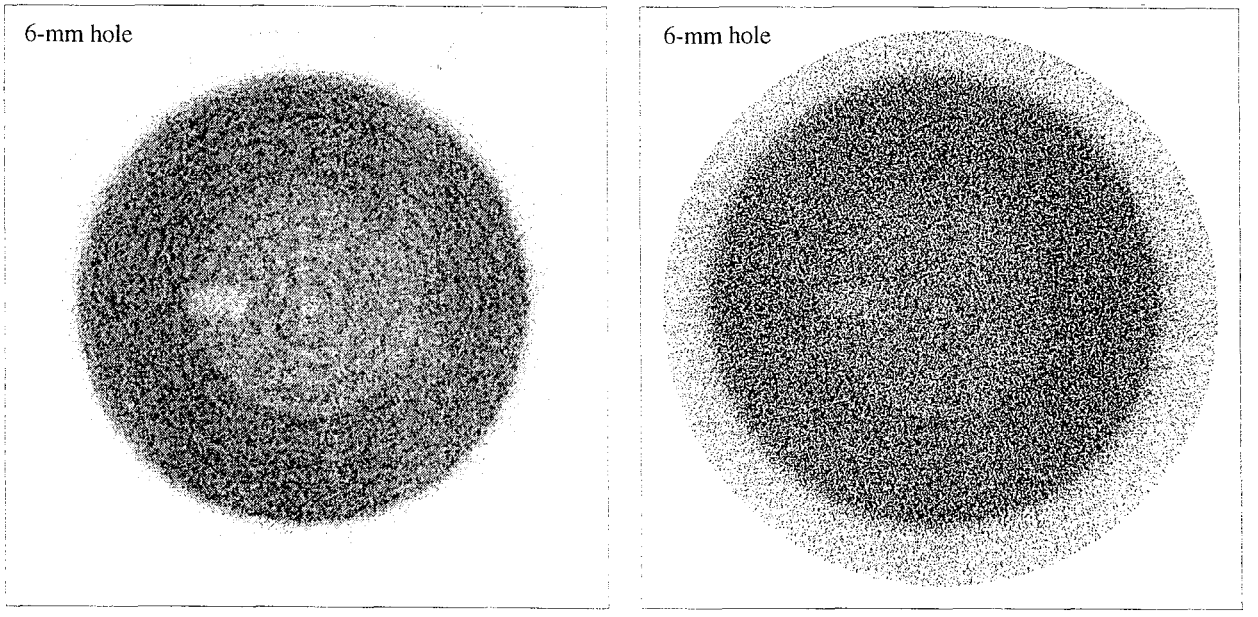

Figure 9. Tomographic reconstruction of thin slice through 6-mm-diameter hole in cylindrical Pb and polyethylene test object done using a Constrained Conjugate Gradient (CCG) algorithm compared to that obtained using a standard Filtered Back Projection (FBP) algorithm. The images are shown at the same contrast level.

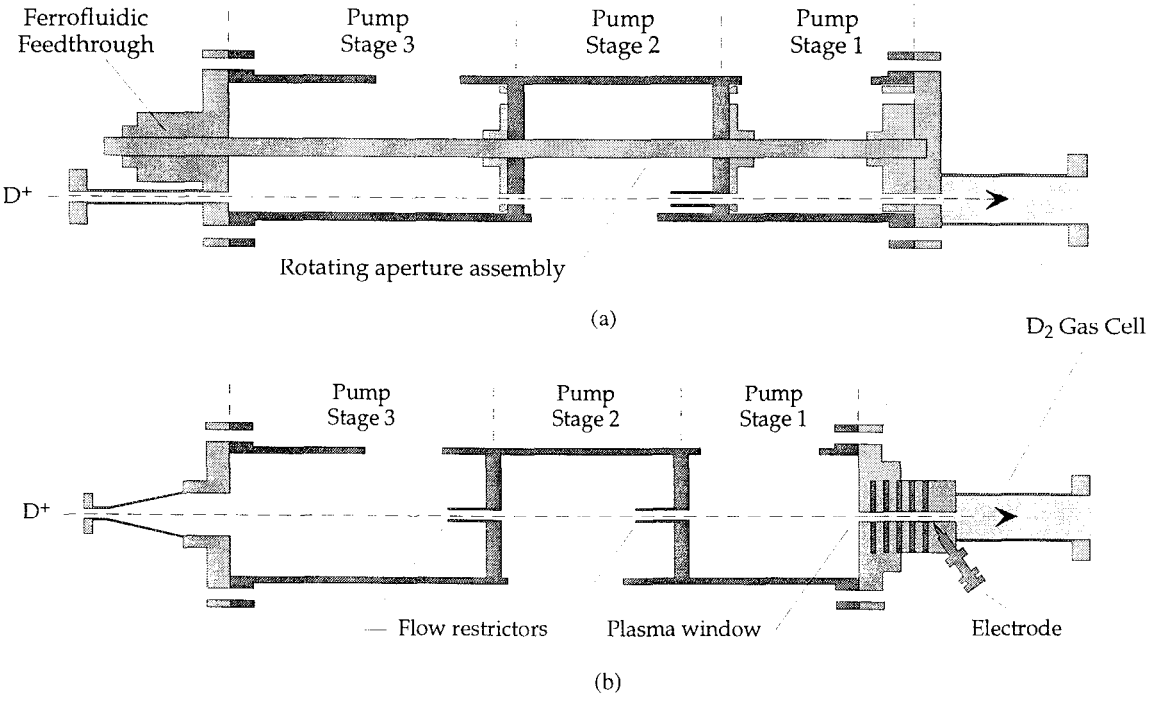

Figure 10. Generalized schematics of "rotating aperture" (a) and "plasma window" (b) D_2 gas target designs currently under development.